JACS
JOURNAL OF THE AMERICAN CHEMICAL SOCIETY
Article
pubs.acs.org/JACS

Tuning the Reactivity of an Actor Ligand for Tandem CO_2 and C−H Activations: From Spectator Metals to Metal-Free

Vincent T. Annibale, Daniel A. Dalessandro, and Datong Song*

Davenport Chemical Research Laboratories, Department of Chemistry, University of Toronto, 80 St. George Street, Toronto, Ontario, Canada, M5S 3H6

Supporting Information

ABSTRACT: The 4,5-diazafluorenide ligand (L^-) serves as an actor ligand in the formal insertion of CO_2 into a C−H bond remote from the metal center. With the Ru(II) complex of L^- as the starting point, Rh(III), Rh(I), and Cu(I) were used as spectator metal centers to tune the reactivity of the actor ligand toward CO_2. In the case of Rh(III)-diazafluorenide a room temperature reversible activation of CO_2 was observed, similar to the isoelectronic Ru(II) analogue. In the case of Rh(I)- and Cu(I)-diazafluorenide CO_2 is trapped by the formation of dinuclear carboxylate complexes and diazafluorene (LH). The spectator metal center could even be replaced entirely with an organic group allowing for the first metal-free reversible tandem CO_2 and C−H activation.

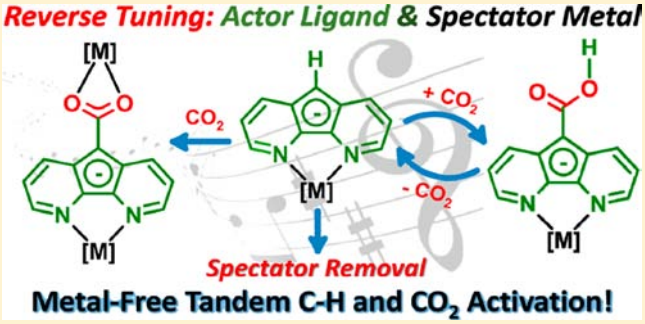

INTRODUCTION

Two fundamental avenues in CO_2 related research are sequestration and utilization. Sequestration has focused on CO_2 storage and gas separation within porous materials.[1−5] CO_2 utilization has focused on reactions where CO_2 is C1 chemical feedstock. For example, in carboxylation reactions the whole CO_2 molecule is incorporated into the product, while in reduction reactions CO_2 can be reduced to a variety of products such as methanol, formic acid derivatives, CO, or methane.[6−11] The major challenge is the remarkable thermodynamic stability of CO_2. Ligand-based reactivity and metal−ligand cooperativity have been highlighted in the recent literature as a new means of small molecule activation.[12−18] Actor ligands that either irreversibly or reversibly activate CO_2 are of particular interest in uncovering new means of CO_2 sequestration and utilization.

One earlier example of a reversible bifunctional activation of CO_2 was described by Braunstein and co-workers.[19−21] Palladium complexes bearing a functional phosphino-enolate ligand $[Ph_2PCHC(O)OEt)_2]^-$ and an anionic C,N-chelate ligand react with CO_2, where CO_2 formally inserts into a C−H bond of the P,O-chelate. It was suggested that the strong σ-donor *trans* to the O-donor might labilize the Pd−O bond and allow the polarized ligand C−H bond to react with CO_2.[19] The Pd(II) center seems to mediate the events leading to this formal insertion and elimination of CO_2 in these P,O-chelate complexes, where the corresponding alkaline metal salts of the phosphino-enolate do not react with CO_2.[22]

Both Milstein and Sanford have recently reported similar reversible pincer ligand-mediated CO_2 activation reactions.[23,24] Both Ru complexes with PNP and PNN pyridine-based pincer ligands demonstrated a new mode of reversible CO_2 activation triggered by ligand aromatization-dearomatization, with concomitant reversible Ru−O and C−C bond formation.[23,24] Recently a Ni(II)-Me complex featuring a doubly deprotonated PNP pincer ligand was prepared by Milstein and co-workers.[25] The electrophilic attack of the complex by CO_2 followed by tautomerization yields a new Ni-bound pincer ligand with an exocyclic methylene arm and a carboxylate on the other pincer arm. There appeared to be little to no direct involvement of the Ni center, unlike the dearomatized PNP and PNN Ru complexes mentioned above.[23,24]

Piers and co-workers examined the reactivity of scandium β-diiminate alkyl complexes toward CO_2.[26] Dimeric complexes were isolated, where CO_2 had inserted into the Sc-alkyl bonds as well as been attacked by the nucleophilic central carbon of the β-diiminate ligand. The highly electropositive Sc(III) center, a potent Lewis acid, and the basic somewhat noninnocent central carbon of the ligand backbone were able to cooperatively activate CO_2. Other examples where the ligand framework plays a major role in the activation of CO_2 include the recent work by Stephan and Sgro with Ru,[27] and Hf[28] phosphinoamide complexes. The Ru tris(aminophosphine) complex reported by Stephan can catalytically perform a ligand-based activation of CO_2, followed by reduction with borane.[27] Similar phosphine ligand-based activation of CO_2 also includes the work of Wass[29] and Erker.[30]

Previously we demonstrated that a zwitterionic Ru(II) 4,5-diazafluorenide complex **1**[31] can activate CO_2.[32] We discovered a formal CO_2 insertion into a ligand C−H bond which occurs

Received: July 18, 2013
Published: September 26, 2013

   dx.doi.org/10.1021/ja4073832 | J. Am. Chem. Soc. 2013, 135, 16175−16183

reversibly at room temperature (Scheme 1).[32] It is worth noting the chemo-selectivity of this process: CO_2 does not

Scheme 1. Reversible Activation of CO_2 by Complex 1[32]

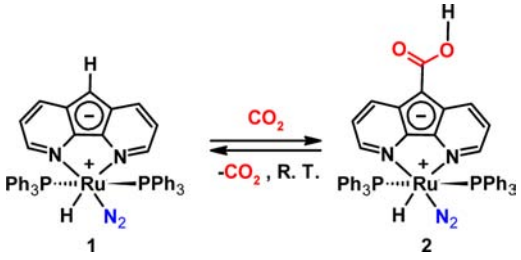

insert into the metal hydride or displace the dinitrogen ligand. The mechanism for the formal insertion of CO_2 into the ligand C−H bond leading to complex **2** likely involves nucleophilic attack of CO_2 by the backbone carbon of diazafluorenide followed by proton migration. The overall process may also be viewed as a reversible tandem CO_2 and C−H activation.

In the reaction of complex **1** with CO_2 diazafluorenide behaves as an actor ligand and reversibly forms a new C−C bond, while the metal center takes on the role of a spectator. The activation of CO_2 occurs at the ligand backbone remote from the metal center where the metal's role is to adjust the acidity of the C−H bond involved in proton migration as well as the strength of the newly formed C−C bond.[32] Unlike the phosphino-enolate[19−21] or pyridine-based pincer[23,24] examples of reversible ligand carboxylation mentioned above, there is no direct involvement of the metal in the Ru diazafluorenide system. The traditional approach taken by inorganic and organometallic chemists is to tune the sterics and electronics of spectator ligands to elicit changes in reactivity at the metal center. As a result of the unusual situation of having an actor ligand that activates CO_2 and a spectator metal center, we report here our explorations into the unconventional approach of tuning the ligand reactivity with different spectator metal centers as well as the successful removal of the spectator metal unit altogether, resulting in metal-free tandem CO_2 and C−H activations.

RESULTS AND DISCUSSION

Rhodium-Diazafluorenide CO_2 Chemistry. We first tested whether the room temperature (RT) reversible ligand-based carboxylation reactivity can be generalized and started by examining the reactivity of the isoelectronic Rh(III) diazafluorenide complex **3** with two triphenylphosphine and two hydride ligands, which we previously synthesized.[33] When dark red-brown complex **3** is placed under an atmosphere of CO_2 an orange-yellow crystalline precipitate of complex **4** forms, where analogous to the Ru(II) system, a formal insertion of CO_2 into the C−H bond in the backbone of the diazafluorenide ligand has occurred (Scheme 2). Complex **4** is insoluble in benzene, toluene, diethyl ether, DME, hexanes, and pentane and has limited solubility in THF.

The X-ray crystal structure of complex **4** is shown in Figure 1 and was obtained by allowing CO_2 to slowly diffuse into a toluene solution of **3**. The Rh(III) center of complex **4** adopts a slightly distorted octahedral geometry and has two *cis*-N-donors from the diazafluorenyl-carboxylic acid ligand, two hydrides *cis* to each other, and two triphenylphosphine ligands *trans* to each other. Complex **4** forms doubly H-bonded dimers in the solid

Scheme 2. Reversible Formal Insertion of CO_2 into Ligand C−H Bond of Complex 3

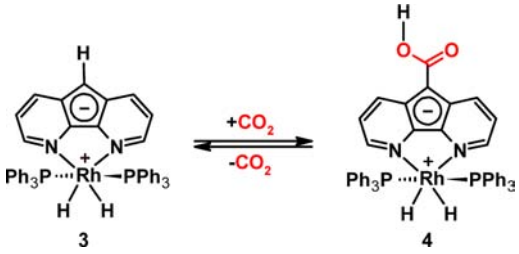

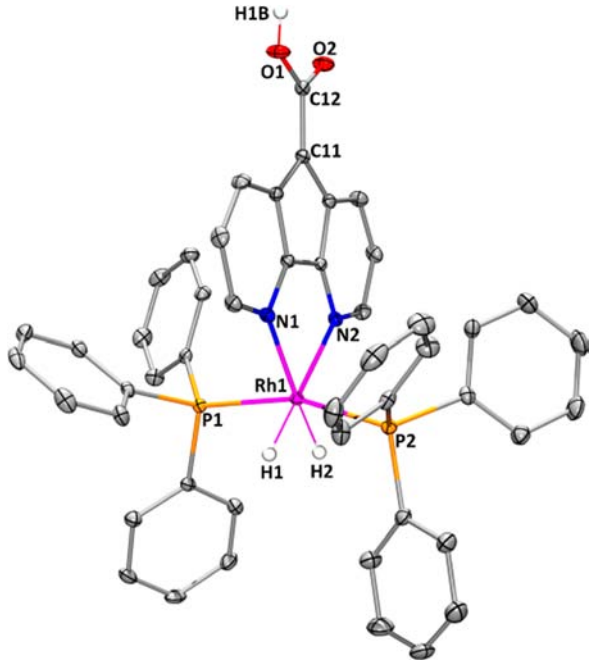

Figure 1. X-ray crystal structure of **4**. Non-hydrogen atoms are shown as 30% probability ellipsoids, the hydrides and carboxylic acid H-atoms are shown as spheres of arbitrary radius, and the rest of the H-atoms are omitted for clarity. Selected bond lengths (Å) and angles (°): Rh1−N1, 2.223(3); Rh1−N2, 2.187(3); Rh1−P1, 2.3200(9); Rh1−P2, 2.2831(9); O1−C12, 1.307(4); O2−C12, 1.267(4); N1−Rh1−N2, 81.53(9); P1−Rh1−P2, 161.26(3); N1−Rh1−P1, 95.64(7); N1−Rh1−P2, 95.54(7); N2−Rh1−P1, 97.00(7); N2−Rh1−P2, 99.48(7); O1−C12−O2, 122.0(3); O1−C12−C11, 117.4(3); O2−C12−C11, 120.5(3).

state, where the O1−O2′ distance is ∼2.58 Å, reminiscent of other carboxylic acids including **2**.[32] In the crystal structure of **4**, it is worth noting that the backbone carbon is sp^2 hybridized and the proton is bound to oxygen. This is in contrast to how other carbanions typically react with CO_2. For instance organometallic reagents such as organolithiums or Grignards typically lack acidic protons and formally undergo an insertion of CO_2 into a C-metal bond to form carboxylates; carboxylic acids form upon the addition of an external acid. For example, the carboxylation of fluorene with CO_2 and K_2CO_3 base gives 9(H)-9-fluorene carboxylate which requires addition of HCl to give 9(H)-9-fluorene carboxylic acid.[34−37] The proton bound to the 9-position of 9(H)-9-fluorene carboxylate does not migrate to the oxygen to give a carboxylic acid group and restore the carbanion. Here the diazafluorenide ligand directly gives a carboxylic acid upon a formal insertion of CO_2 into the C−H bond without the addition of external acid. In addition, the

dx.doi.org/10.1021/ja4073832 | J. Am. Chem. Soc. 2013, 135, 16175−16183

decarboxylation of metal carboxylates formed from the reaction of Grignards or organolithium reagents and CO_2 typically requires forcing conditions, while the decarboxylation of **4** occurs readily at ambient temperature to give **3** upon removal of CO_2 atmosphere.

When an analytically pure sample of complex **4** was partially dissolved in THF-d_8, under N_2 atmosphere, the initially yellow suspension gives an orange solution after sitting at RT overnight. $^1H\{^{31}P\}$ and ^{31}P NMR spectroscopy revealed that a mixture of **3** and **4** forms (~2.3:1 ratio), where the major species is **3**. The ratio of **3** to **4** does not change significantly even after an additional 24 h in a sealed J. Young tube. The decarboxylation can be driven to completion by doing three cycles of dissolving in THF under N_2 and pumping away the volatiles under vacuum. Replacing the dinitrogen atmosphere inside the J. Young tube with CO_2 affords clean conversion to **4** and allows for ^1H and ^{31}P NMR characterization. In the $^1H\{^{31}P\}$ NMR spectrum the hydrides of **4** appear as a doublet at −16.72 ppm, and in the ^{31}P NMR spectrum the triphenylphosphine ligands of **4** display a doublet at 47.95 ppm with J_{Rh-P} = 117.1 Hz.

The isoelectronic Ru(II) and Rh(III) diazafluorenide complexes react with CO_2 in an analogous way, both engaging in RT reversible formal insertion of CO_2 into the remote ligand C−H bond. To further tune the electronics of the diazafluorenide ligand, we decided to look at the effect of changing the metal's oxidation state, going from Rh(III) to the more electron-rich Rh(I). When the Rh(I) diazafluorenide bis(triphenylphosphine) complex,[33] **5**, is dissolved in benzene and placed under CO_2, the initially olive-green colored solution turns red instantly. The red solution displayed two equal intensity doublets at ~56 and 51 ppm in the ^{31}P NMR spectrum suggestive of two inequivalent $\{Rh(PPh_3)_2^+\}$ units. X-ray crystallography revealed the molecular structure of **6** (Figure 2) as a dinuclear Rh(I) species where the two Rh(I) centers are bridged by a novel diazafluorenyl-carboxylate ligand, and the mother liquor contained diazafluorene as judged by ^1H NMR (Scheme 3).

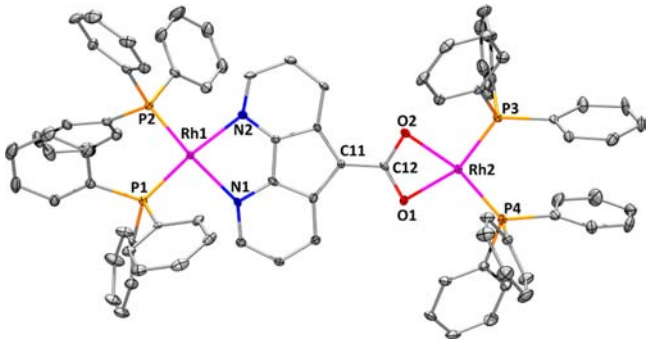

Figure 2. X-ray crystal structure of **6**. Non-hydrogen atoms are shown as 30% probability ellipsoids, and the H-atoms along with the five benzene solvent molecules are omitted for clarity. Selected bond lengths (Å) and angles (°): Rh1−P1, 2.2331(15); Rh1−P2, 2.2289(15); Rh1−N1, 2.187(5); Rh1−N2, 2.164(5); Rh2−O1, 2.141(4); Rh2−O2, 2.129(4); Rh2−P3, 2.1845(16); Rh2−P4, 2.1807(16); O1−C12, 1.292(7); O2−C12, 1.301(6); P1−Rh1−P2, 99.54(6); N1−Rh1−N2, 82.60(17); P1−Rh1−N1, 91.50(12); P2−Rh1−N2, 92.28(13); O1−Rh2−O2, 62.61(14); P3−Rh2−P4, 98.48(6); O1−Rh2−P4, 103.17(11); O2−Rh2−P3, 95.67(11); O1−C12−O2, 117.6(5); O1−C12−C11, 122.6(5); O2−C12−C11, 119.7(5).

Scheme 3. Reactivity of 5 Towards CO_2 and Possible Pathway for the Formation of 6

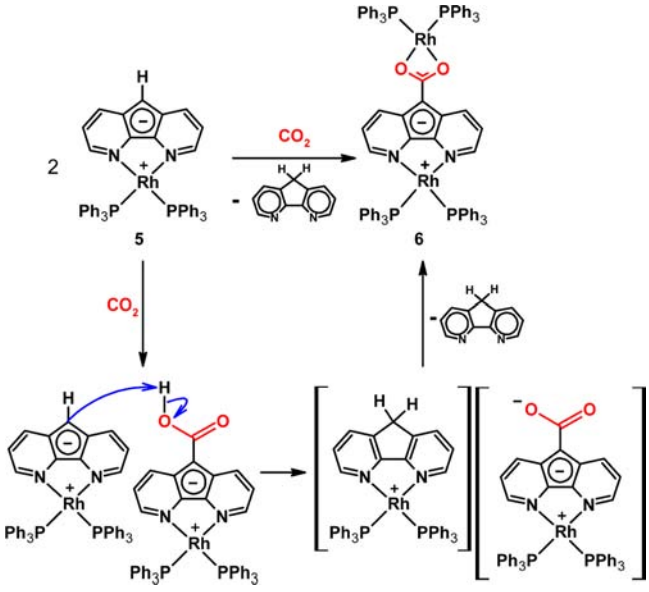

Each of the two Rh(I) centers in complex **6** adopts a distorted square-planar coordination geometry where Rh1 is coordinated to the two N-donor atoms of the diazafluorenyl moiety and two P-donor atoms of two PPh_3 ligands, while Rh2 is coordinated to the two O-donor atoms of the carboxylate moiety and two P-donor atoms of two PPh_3 ligands. Repulsion between the two phosphine ligands bound to Rh1 causes the two phosphorus donor atoms P1 and P2 to reside on different sides of the plane defined by the five-membered chelate ring. The dihedral angle between the plane defined by N1−Rh1−N2 and the plane defined by P1−Rh1−P2 is ~26°. Similar repulsion between the two phosphine ligands has been observed previously in the Rh(I) diazafluorenide starting material complex **5**.[33] The plane of CO_2-derived carboxylate moiety deviates slightly from the plane of diazafluorenyl moiety where the dihedral angle is ~11°. The tuning of diazafluorenide actor ligand with a more electron rich Rh(I) metal center compared with Rh(III) leads to an increased basicity of the carbanionic backbone, which is able to deprotonate the carboxylic acid resulting from the reaction between another molecule of **5** and CO_2 (see Scheme 3). This gives a Rh(I)-diazafluorene and a Rh(I)-diazafluorenyl-carboxylate intermediate. The subsequent substitution of the neutral diazafluorene ligand by the Rh(I)-bound diazafluorenyl-carboxylate gives the dinuclear complex **6**. The CO_2 release can no longer occur under ambient conditions because CO_2 is trapped by the second metal center, and the absence of proton on O that can engage in proton transfer prevents the facile decarboxylation.

Copper-Diazafluorenide CO_2 Chemistry. Previously our group had synthesized a Cu(I) N-heterocyclic carbene (NHC) complex with a phosphine-functionalized diazafluorenide ligand which can engage in ligand transfer to Rh(I) or Au(I) to form macrocyclic complexes.[38] The Cu-NHC phosphine-functionalized diazafluorenide complex existed as a monomer in solution and a dimer in the solid state. Cu(I)-NHC complexes[39,40] have emerged as carboxylation[41−43] and CO_2 reduction catalysts.[44] We decided to compare the reactivity of Rh(I) and Cu(I) diazafluorenide complexes, which are both low valent electron-rich systems. The deep purple Cu(I)-

dx.doi.org/10.1021/ja4073832 | J. Am. Chem. Soc. 2013, 135, 16175−16183

diazafluorenide complex **7** was prepared straightforwardly from the reaction of NaL and Cu(IPr)Cl. Complex **7** is soluble in THF, DME, benzene, toluene, and DMSO and is slightly soluble in hexanes. The X-ray crystal structure of **7** is shown in Figure 3. Complex **7** exhibits a monomeric three-coordinate

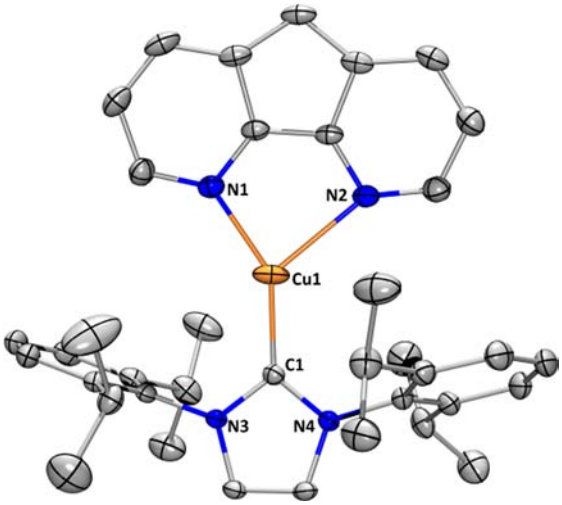

Figure 3. X-ray crystal structure of **7**. Non-hydrogen atoms are shown as 30% probability ellipsoids, and H-atoms are omitted for clarity. Selected bond lengths (Å) and angles (°): Cu1−C1, 1.886(3); Cu1−N1, 2.014(3); Cu1−N2, 2.307(3); N1−Cu1−N2, 84.88(10); C1−Cu1−N1, 147.42(12); C1−Cu1−N2, 127.45(11).

structure where the Cu(I) center adopts a distorted Y-shaped geometry and is bound to two N-donors from the diazafluorenide ligand and the carbene C-donor. The Cu1−N1 bond length is 2.014(3) Å, while the Cu1−N2 bond length is significantly longer at 2.307(3) Å. The sum of the angles around the Cu1 center is 359.8(1)° indicating a planar geometry. The diazafluorenide ligand and the five-membered imidazolylidene ring of the bulky IPr ligand are almost coplanar, the dihedral angle between the two planes is only ∼11°. Thompson and co-workers also observed a similar orientation of IPr relative to bidentate neutral or anionic *N,N*-chelate ligands,[45] as opposed to the typical perpendicular orientation.[41,46,47] The ^{1}H NMR in C_6D_6 for complex **7** revealed that the backbone proton at the 9-position of the L^- ligand appeared as a singlet at 6.59 ppm.

When a toluene solution of complex **7** was placed under an atmosphere of CO_2 a yellow microcrystalline precipitate of complex **8** formed (Scheme 4). Once again we have an example of a formal insertion of CO_2 into the diazafluorenide backbone C−H bond. The X-ray quality crystals of **8** were obtained from slow diffusion of CO_2 into a toluene solution of **7**, and the molecular structure of **8** is shown in Figure 4. Similar to complex **7** the crystal structure of complex **8** shows that the Cu(I) center adopts a three-coordinate Y-shaped geometry. The Cu1−N1 bond length is 2.0529(19) Å, while the Cu1−N2 bond length is significantly longer at 2.2177(19) Å. The sum of the angles around the Cu1 center is 359.37(9)° indicating a planar geometry. The diazafluorenyl plane and the five-membered imidazolylidene ring of the bulky IPr ligand are almost coplanar with the dihedral angle between the two planes of ∼15°. Complex **8** forms doubly H-bonded dimers in the solid state where the O1−O2′ distance is ∼2.59 Å similar to what was noted previously with other carboxylic acids.

Scheme 4. Reactivity of Complex 7 Towards CO_2, Giving Complex 8 as the Kinetic Product and Complex 9 as the Thermodynamic Product

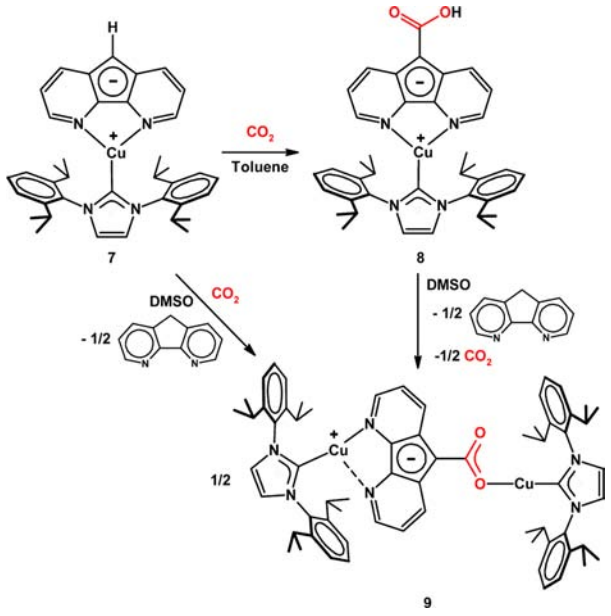

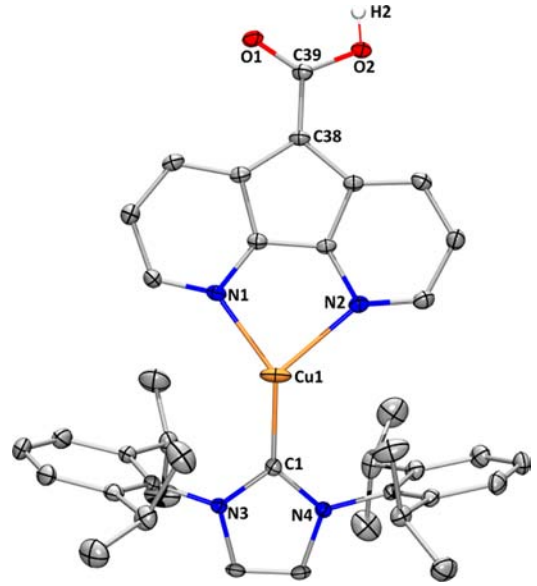

Figure 4. X-ray crystal structure of **8**. Non-hydrogen atoms are shown as 30% probability ellipsoids, the carboxylic acid H-atom is shown as a sphere of arbitrary radius, and the rest of the H-atoms along with the toluene solvate are omitted for clarity. Selected bond lengths (Å) and angles (°): Cu1−C1, 1.880(2); Cu1−N1, 2.0529(19); Cu1−N2, 2.2177(19); O1−C39, 1.251(3); O2−C39, 1.324(3); N1−Cu1−N2, 85.54(7); C1−Cu1−N1, 142.25(9); C1−Cu1−N2, 131.58(8); O1−C39−O2, 121.6(2); O1−C39−C38, 122.7(2); O2−C39−C38, 115.6(2).

The reversibility of the carboxylation was examined by partially dissolving analytically pure complex **8** in THF under N_2 atmosphere, resulting in a drastic color change from a bright yellow-orange suspension to a pink-purple solution. The major species upon removal of THF and dissolving the resulting purple residue in C_6D_6 was a complex with two different IPr environments as evidenced by the presence of two equal intensity heptets for the $-C\underline{H}(CH_3)_2$ protons at 2.78 and 2.62

dx.doi.org/10.1021/ja4073832 | J. Am. Chem. Soc. 2013, 135, 16175−16183

ppm. Only a minor amount of decarboxylated complex **7** had reformed where the heptet belonging to $-C\underline{H}(CH_3)_2$ protons of **7** appears at 2.69 ppm. When DMSO-d_6 was used as the solvent to study the reversibility of the carboxylation by dissolving **8** under N_2 atmosphere, instead of complex **7**, a bright pink precipitate **9** formed after standing overnight at RT. ^{1}H NMR spectroscopy revealed that only LH remained in the DMSO-d_6 supernatant. The same result of a pink precipitate **9** and an LH solution was also observed when a DMSO-d_6 solution of **7** was reacted with 1 atm of CO_2. The molecular structure of complex **9** has been confirmed by X-ray crystallography (Figure 5). Complex **9** is a dinuclear Cu(I)-

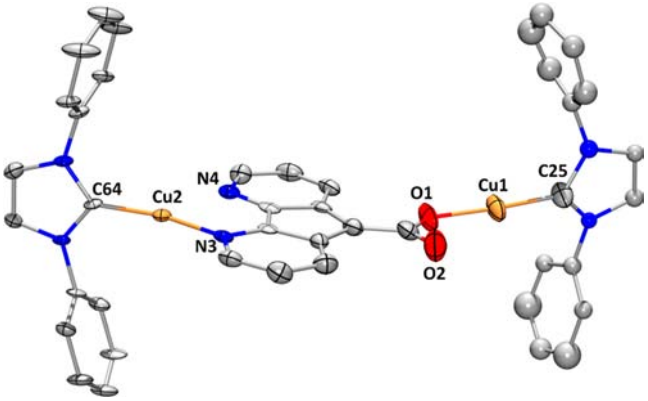

Figure 5. X-ray crystal structure of **9**. Non-hydrogen atoms are shown as 30% probability ellipsoids except for disordered portions of the IPr ligand on the right. Only one component of the disordered IPr ligand and Cu2 is shown. The isopropyl groups on the IPr ligands and H-atoms are removed for clarity. Selected bond lengths (Å) and angles (°):Cu1−O1, 1.820(3); Cu1−C25, 1.850(4); Cu2−C64, 1.887(3); Cu2−N3, 1.931(3); Cu2−N4, 2.556(3); O1−Cu1−C25, 172.08(19); N3−Cu2−C64, 162.87(14).

IPr complex where the two $\{Cu(IPr)^+\}$ units are bridged by a dianionic diazafluorenyl-carboxylate ligand similar to complex **6** above. In the solid state both copper centers are two-coordinate with O1−Cu1−C25 and N3−Cu2−C64 angles of 172.08(19)° and 162.87(14)°, respectively. The two IPr ligands adopt a perpendicular orientation relative to the central diazafluorenyl-carboxylate ligand. The ^{1}H NMR spectrum of complex **9** revealed a symmetrical structure in solution with three sets of diazafluorenyl resonances, hinting that the unsymmetrical structure in the solid state is likely due to crystal packing effects. Complex **9** is soluble in THF, DME, benzene, and toluene but insoluble in DMSO, pentane, and hexanes.

Complex **8** represents the kinetic product of CO_2 activation by complex **7** and can be isolated because of its poor solubility in nonpolar solvents such as toluene. Complex **9** and free LH represent the thermodynamic products of CO_2 activation, which can form when an equimolar amount of acidic complex **8** is deprotonated by basic complex **7** in solution. Complex **9** can form upon either partial carboxylation of **7** under CO_2 atmosphere or partial decarboxylation of **8** under N_2 atmosphere at RT.

Metal-Free Tandem CO_2 and C−H Activation. Given that the metal played a spectator role in the tandem CO_2 and C−H activation noted for the Ru, Rh, Cu, systems above, we decided to explore whether the spectator could be removed altogether and examined metal-free systems. We envision that the alkylation of a nitrogen atom of diazafluorenide can create a formal positive charge on the nitrogen atom, which may play a similar role as the positively charged spectator metal units. To test our hypothesis, we turned to N-methylated diazafluorenide derivative **10**, where two possible resonance structures (charge separated **10** and combined **10′**) are shown in Scheme 5.

Scheme 5. Synthesis of Compound 10 and Reversible Metal-Free Tandem CO_2 and C−H Activation

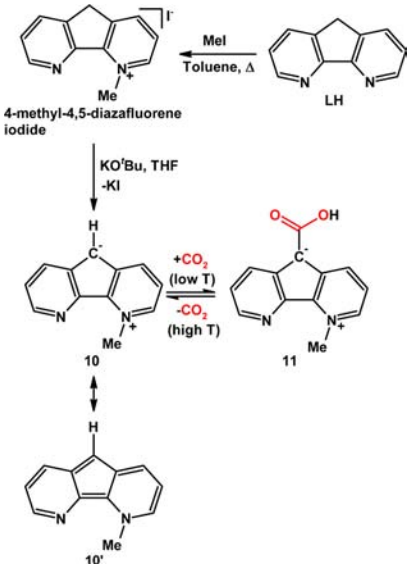

Compound **10** was prepared from diazafluorene through sequential N-methylation with MeI and deprotonation with KO*t*Bu. Compound **10** is soluble in THF, toluene, DME, and DMSO and is sparingly soluble in hexanes or pentane. Compound **10** in solution is stable toward air and moisture for a few hours but decomposes to an intractable mixture after several days. The crystal structure of **10** is shown in Figure 6. The methylated pyridyl nitrogen N2 is trigonal planar with the sum of the angles around N2 of 360.0(1)°. The ^{1}H NMR in

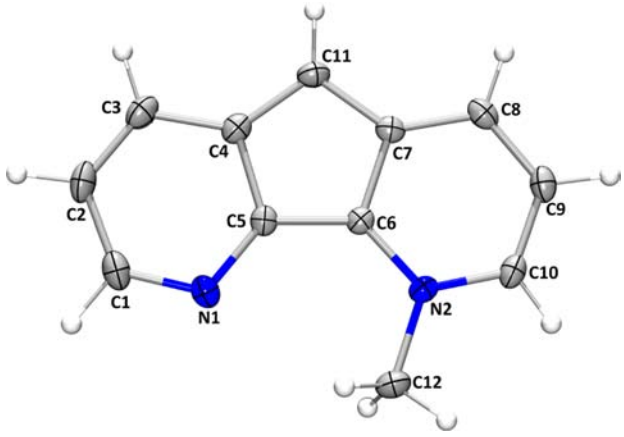

Figure 6. X-ray crystal structure of **10**. Non-hydrogen atoms are shown as 30% probability ellipsoids, H-atoms are shown as spheres of arbitrary radius. Only one of the molecules of **11** from the asymmetric unit is represented. Selected bond lengths (Å) and angles (°): C4−C11, 1.396(2); C7−C11, 1.405(2); N2−C6, 1.3624(19); N2−C10, 1.340(2); N2−C12, 1.4733(19); C4−C11−C7, 107.64(14); C6−N2−C10, 120.54(14); C6−N2−C12, 119.76(13); C10−N2−C12, 119.70(14).

dx.doi.org/10.1021/ja4073832 | J. Am. Chem. Soc. 2013, 135, 16175−16183

DMSO-d_6 revealed an unsymmetrical structure where each of the six pyridyl protons of the diazafluorenyl moiety has a distinct chemical shift. The backbone proton at the 9-position appears as a singlet at 6.42 ppm, and the methyl group protons appear as a singlet at 4.97 ppm.

When a DMSO-d_6 solution of **10** was placed under a CO_2 atmosphere at RT, only a trace amount of the carboxylation product can be observed by ^{1}H NMR spectroscopy. Surprisingly upon freezing the solution in an ice water bath, there was an instantaneous color change from blue-violet to red-violet, and the ^{1}H NMR revealed that the majority of the starting material had been consumed and converted to compound **11**. Once again a formal insertion of CO_2 into C−H bond has occurred; however the insertion requires a temperature lower than RT in order to occur to an appreciable extent, possibly to overcome the entropic barrier of the reaction. After addition of CO_2 and chilling the DMSO-d_6 solution in ice water, the diagnostic peak at 6.42 ppm belonging to the backbone proton at the 9-position for compound **10** diminishes, and an acidic proton peak at 11.15 ppm appears; all the pyridyl protons in compound **11** are downfield shifted versus their counterparts in compound **10**. The newly formed carboxylic acid carbon peak appears in the ^{13}C NMR spectrum at 167.95 ppm. The molecular structure of compound **11** has been confirmed by X-ray crystallography (Figure 7). The

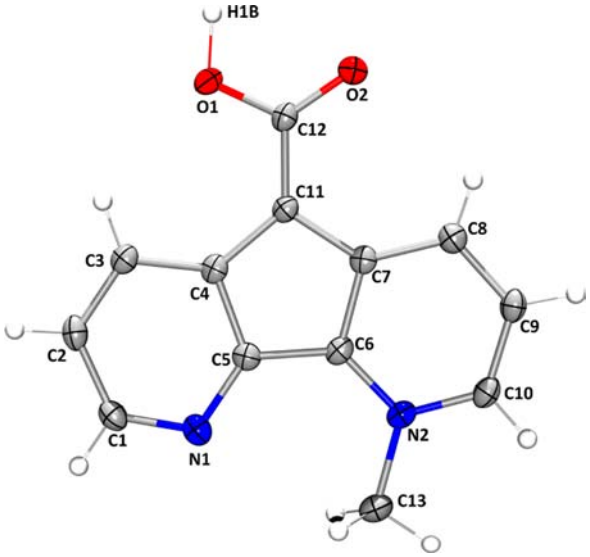

Figure 7. X-ray crystal structure of **11**. Non-hydrogen atoms are shown as 30% probability ellipsoids, H-atoms are shown as spheres of arbitrary radius. Selected bond lengths (Å) and angles (°): C4−C11, 1.424(3); C7−C11, 1.427(3); C11−C12, 1.415(3); O1−C12, 1.328(2); O2−C12, 1.261(2); N2−C6, 1.359(2); N2−C10, 1.341(3); N2−C13, 1.480(3); C4−C11−C7, 107.29(17); C4−C11−C12, 128.93(18); C7−C11−C12, 123.62(17); O1−C12−O2, 120.83(18); O2−C12−C11 122.99(18); O1−C12−C11, 116.18(17).

carboxylic acid group and the diazafluorenyl moiety are nearly coplanar with the dihedral angle of ∼5°. Compound **11** forms doubly H-bonded dimers in the solid state where the O1−O2′ distance is ∼2.57 Å similar to other carboxylic acids and complexes **2**, **4**, and **8**, above.

To test the reversibility of the formal CO_2 insertion, a sample of **11** was dissolved in DMSO-d_6 under N_2 atmosphere in a sealed NMR tube. This gave partial decarboxylation after overnight at RT where the ratio of compound **11** to **10** is ∼2.2:1 according to ^{1}H NMR spectrum. After heating at 50 °C for 10 min decarboxylation occurs, and the only visible species by ^{1}H NMR is **10**. When the solution is rechilled in ice water, CO_2 in the headspace of the NMR tube is recaptured, and **11** becomes the major product (ratio of compounds **11** to **10** is ∼7.5:1). Although there have been several developments in metal-free and main-group CO_2 activation,[48−62] compound **10** is the first example of a metal-free system capable of reversible tandem CO_2 and CH activations. The TGA curve of a solid sample of **11** displays a 19.70% weight loss between 126 and 147 °C, which could be attributed to the loss of CO_2. The remainder of the TGA curve for compound **11** above ∼150 °C appears similar to that of compound **10** (see Supporting Information).

■ CONCLUSIONS

In summary, we have shown that the mode of CO_2 activation by the actor diazafluorenide ligand can be tuned by varying the spectator metal center. A RT reversible formal insertion of CO_2 into a remote ligand C−H bond was studied where the spectator metal's role is likely to modulate the strength of the resulting C−C bond and adjust the acidity of the C−H bond to allow the carboxylation and decarboxylation to occur readily at RT. Tuning the metal via oxidation state (e.g., Rh^{III} vs Rh^{I}) gave markedly different results in ligand-based reactivity. In the case of Rh(III) both carboxylated **4** and decarboxylated **3** can coexist in solution, while in the case of Rh(I) the acid that likely generated *in situ* is instantly deprotonated by complex **5** to form the dinuclear complex **6** and diazafluorene. In the case of Cu(I), the kinetic product of CO_2 activation is the acid **8** which can be isolated as a precipitate from nonpolar solvents, while the thermodynamic products are the dinuclear complex **9** and diazafluorene. The spectator metal unit could also be replaced entirely with an organic group; the resulting metal-free compounds **10** and **11** can engage in reversible equimolar CO_2 capture (involving tandem CO_2 and CH activation) and release. Current efforts are focused on catalytic applications of this ligand-based and metal-free reactivity as well as establishing the scale of the electronic effects of various spectator metal centers.

■ EXPERIMENTAL SECTION

General Information. All air- or moisture-sensitive operations were performed using Schlenk/vacuum-line techniques under either dinitrogen or carbon dioxide or in a dinitrogen atmosphere glovebox from MBraun. Complexes **3**,[33] **5**,[33] and Cu(IPr)Cl[63−65] were prepared from literature procedures. 4,5-Diazafluorene[66,67] was synthesized from literature procedures, and 4-methyl-4,5-diazafluorene iodide[68] was prepared from a modified literature procedure where toluene was used as the solvent instead of benzene. Compound **10** is reported previously;[69] here an alternative synthesis, reactivity, NMR data, and an X-ray crystal structure are reported. All glassware was dried overnight in a 180 °C oven prior to use except for J. Young NMR tubes which were dried overnight in a 60 °C oven. Carbon dioxide was purchased from Linde (Grade 4.0). THF, benzene, DME, THF-d_8, and benzene-d_6 were dried over Na/benzophenone and either distilled under nitrogen or vacuum-transferred before use. Toluene, pentane, and hexanes were dried after passing through a Pure Solv Innovative Technology Grubbs'-type solvent purification system and degassed through three consecutive freeze−pump−thaw cycles. DMSO and DMSO-d_6 were dried over CaH_2 at 80 °C overnight and vacuum distilled prior to use. IR spectra were collected on a Perkin-Elmer Spectrum One FT-IR spectrometer. Thermogravimetric analyses (TGA) were performed on a TA Instruments SDT Q600 instrument under dinitrogen atmosphere with a heating rate of 10 °C per minute.

dx.doi.org/10.1021/ja4073832 | J. Am. Chem. Soc. 2013, 135, 16175−16183

^{1}H, ^{31}P, and ^{13}C NMR spectra were recorded on a Varian 400 MHz, Bruker Avance III 400 MHz, or Agilent DD2−600 MHz NMR spectrometer. All chemical shifts are reported in ppm relative the residual protio-solvent peaks, and ^{31}P NMR is referenced externally using 85% H_3PO_4 in a flame-sealed capillary. Elemental analyses were performed by ANALEST at the University of Toronto.

Synthesis of **4**. In the glovebox, 50 mg (0.062 mmol) of **3** was dissolved in 9 mL of toluene to give a red-brown solution which was placed inside a Pyrex solvent bomb with resealable Teflon valve and removed from the glovebox. The mixture was degassed via two freeze−pump−thaw cycles, and then 1 atm of CO_2 was introduced, and the bomb was sealed. After sitting under CO_2 atmosphere overnight (no stirring) yellow crystals resulted. The bomb was brought back into the glovebox for workup where it was degassed briefly by opening to vacuum, the yellow-orange crystals of **4** were quickly collected by filtration and washed with hexanes and dried under high vacuum (50 mg, 95% yield). Crystals of **4** suitable for X-ray crystallographic analysis were grown under CO_2 from toluene, by allowing CO_2 to diffuse slowly into a septum-sealed vial containing a toluene solution of **3**.

A 9 mg sample of bright orange **4** was partially dissolved in 0.6 mL of THF-d_8, filtered, and placed in a J. Young tube. After overnight at RT the initially bright yellow solution appears orange, and the ^{1}H{^{31}P} and ^{31}P NMR spectra were recorded, revealing a mixture of **3** and **4**.[70] The J. Young tube was then degassed via two freeze−pump−thaw cycles, and CO_2 (1 atm) was introduced at RT. Immediately after introduction of CO_2 the solution appears bright yellow, and after approximately 10 min the ^{1}H{^{31}P} and ^{31}P NMR spectra were recorded revealing the presence of **4**. ^{13}C NMR could not be obtained due to poor solubility of **4** in THF-d_8. ^{1}H{^{31}P} NMR under CO_2 (400 MHz, 25 °C, THF-d_8, δ): 9.42 (s, 1H), 8.12 (d, J = 7.9 Hz, 2H), 7.63 (d, J = 7.6 Hz, 2H), 7.29−7.05 (m, 30H), 6.56 (dd, J = 5.0 Hz, J = 7.9 Hz, 2H), −16.72 (d, J = 17.3 Hz, 2H). ^{31}P NMR under CO_2 (161.8 MHz, 25 °C, THF-d_8, δ): 47.95 (d, J_{Rh-P} = 117.1 Hz, 2P). IR (nujol mull): ν(C═O), 1608 cm^{-1} (s). Anal. calcd for ($C_{48}H_{39}N_2O_2P_2Rh$): C, 68.58; H, 4.68; N, 3.33. Found: C, 68.79; H, 5.00; N, 3.20.

Synthesis of **6**. In the glovebox, 95 mg (0.120 mmol) of **5** was dissolved in 4 mL of benzene to give an olive-green solution/suspension which was placed inside a Pyrex solvent bomb with resealable Teflon valve and removed from the glovebox. The mixture was degassed via two freeze−pump−thaw cycles, and then 1 atm of CO_2 was introduced, and the bomb was sealed, within 1 h a dark red solution results. The bomb was left to sit without agitation (no stirring) for 14 days. After 14 days red-orange crystals of **6**·5(C_6H_6) suitable for X-ray crystallographic analysis resulted with a pale reddish-brown supernatant. In the glovebox, the solution was briefly degassed by opening to vacuum, and the red-orange crystals were quickly collected by filtration, washed with a small amount of benzene and pentane, and dried under vacuum (71 mg, 79% yield based on **6**·0.66(C_6H_6)). The volatiles were removed from the filtrate and analyzed by ^{1}H and ^{31}P NMR in C_6D_6 to show the presence of LH along with some triphenylphosphine oxide. Poor solubility prevented a ^{13}C NMR spectrum for **6** from being obtained. ^{1}H NMR (400 MHz, DMSO-d_6, δ): 7.86 (m, 2H), 7.72 (m, 12H), 7.47 (m, 12H), 7.36 (s, residual C_6H_6), 7.29 (m, 12H), 7.16 (m, 24H), 6.58 (m, 4H). ^{31}P NMR (162 MHz MHz, DMSO-d_6, δ): 56.23 (d, 2P, J_{Rh-P} = 193.5 Hz), 50.71 (d, J_{Rh-P} = 187.7 Hz, 2P). Anal. calcd for ($C_{84}H_{66}N_2O_2P_2Rh_2$)·0.66($C_6H_6$) (note: ratio of **6** to C_6H_6 determined from integration of ^{1}H NMR spectrum): C, 69.66; H, 4.65; N, 1.85. Found: C, 69.84; H, 4.89; N, 1.82. IR (nujol mull): ν(C═O) 1554 cm^{-1}, 1434 cm^{-1}.

Synthesis of **7**. In the glovebox, to a suspension of 28 mg (0.71 mmol) of 60% NaH as a dispersion in mineral oil in 3 mL of THF was added (dropwise) 3 mL of a THF solution containing 71 mg (0.42 mmol) of LH, and this was stirred for 20 min to give a deep purple-pink solution of NaL. The NaL solution/suspension was filtered through a microfrit plug to remove excess NaH and added dropwise to a stirring solution containing 205 mg (0.42 mmol) of Cu(IPr)Cl in 5 mL of THF. After the addition of NaL was complete a dark purple solution resulted. After 10 min the volatiles were removed under vacuum, and the residue was extracted with toluene and filtered through Celite. Removal of the toluene under vacuum results in the formation of analytically pure, X-ray diffraction quality crystals. The dark purple crystals were dried in vacuum (235 mg, 90% yield). ^{1}H NMR (400 MHz, C_6D_6, δ): 8.07 (dd, J = 1.1 Hz, J = 8.2 Hz, 2H), 7.36 (t, J = 7.8 Hz, 2H), 7.17 (d, J = 7.9 Hz, 4H), 7.02 (dd, J = 4.5 Hz, J = 8.2 Hz, 2H), 6.83 (d, J = 4.2 Hz, 2H), 6.59 (s, 1H), 6.37 (s, 2H), 2.69 (hept, J = 6.6 Hz, J = 13.6 Hz, 4H), 1.18 (d, J = 6.8 Hz, 12H), 1.09 (d, J = 6.9 Hz, 12H). ^{13}C NMR (100 MHz, C_6D_6, δ): 146.20, 138.90, 136.28, 131.96, 130.40, 129.32, 126.31, 124.48, 122.55, 117.30, 79.87, 29.10, 25.04, 23.69. Anal. calcd for ($C_{38}H_{43}N_4Cu$): C, 73.69 ; H, 7.00 ; N, 9.05. Found: C, 73.96; H, 7.51; N, 8.69.

Synthesis of **8**. In the glovebox, 95 mg (0.15 mmol) of **7** was dissolved in 6 mL of toluene to give a deep purple solution which was placed inside a Pyrex solvent bomb with resealable Teflon valve and removed from the glovebox. The mixture was degassed via two freeze−pump−thaw cycles, and then 1 atm of CO_2 was introduced, and the bomb was sealed. After sitting under CO_2 atmosphere overnight (no stirring) at RT yellow-orange crystals along with a pale pink, almost colorless, supernatant resulted. The bomb was brought back into the glovebox for workup where it was degassed briefly by opening to vacuum. The yellow-orange crystals of **8**·(PhMe) were quickly collected by filtration and washed with hexanes and dried under high vacuum (86 mg, 80% yield based on (**8**)·0.5(PhMe)). Crystals of **8**·(PhMe) suitable for X-ray crystallographic analysis were grown under CO_2 from toluene, by allowing CO_2 to diffuse slowly into a septum-sealed vial containing a toluene solution of **7**. The behavior of complex **8** in solution prevented solution-based NMR characterization. Anal. calcd For ($C_{39}H_{43}N_4O_2Cu$)·0.5(C_7H_8): C, 71.96; H, 6.68; N, 7.90. Found: C, 71.45; H, 6.95; N, 7.94. IR (nujol mull): ν(C═O) 1580 cm^{-1}, 1603 cm^{-1}.

Synthesis of **9**. *Method A.* In the glovebox, 120 mg (0.19 mmol) of **7** was dissolved in 5 mL of DMSO to give a deep purple solution which was placed inside a Pyrex solvent bomb with resealable Teflon valve and removed from the glovebox. The mixture was degassed via two freeze−pump−thaw cycles, and then 1 atm of CO_2 was introduced, and the bomb was sealed. After sitting under CO_2 atmosphere overnight (no stirring) at RT a pink precipitate of **9** resulted. The bomb was brought back into the glovebox for workup where it was degassed briefly by opening to vacuum. The pink precipitate was quickly collected by filtration and washed with DMSO, and the precipitate was dissolved in DME (∼2 mL). Vapor diffusion of hexanes into the DME solution of **9** over 1 week resulted in pink crystals of **9**·2(DMSO)·(DME) which were collected by filtration, washed with hexanes, and dried under high vacuum (94 mg, 78% crystalline yield based on (**9**)·2(DMSO)·0.28(DME)). The product formed by method A contained a small amount of **7** by ^{1}H NMR, and method B was used to obtain an analytically pure compound for elemental analysis.

Method B. In the glovebox, 289 mg (0.40 mmol) of (**8**)·0.5(C_7H_8) was dissolved/suspended in 3 mL of DMSO in a 20 mL scintillation vial, the initially bright orange suspension gradually turned pink, and a small amount of gas evolution was observed. The pink suspension in the sealed vial was stirred at RT overnight. The resulting pink precipitate was collected by filtration and washed with DMSO, the pink precipitate was dissolved in DME (∼1 mL), and placed inside the −35 °C freezer. After 2 days at −35 °C a pink precipitate formed from the cold DME, the supernatant was quickly pipetted off, and the pink precipitate was redissolved in DME (∼2 mL). Vapor diffusion of pentane into the DME solution of **9** gave pink crystals suitable of EA that were collected by filtration, washed with pentane, and dried under vacuum (117 mg, 44% yield based on **9**·2(DMSO)·0.28(DME). X-ray diffraction quality crystals were obtained after a second recrystallization from vapor diffusion of pentane into benzene solution of **9**. ^{1}H NMR (600 MHz, 25 °C, C_6D_6, δ): 9.08 (dd, J = 8.2, 1.3 Hz, 2H), 7.28 (t, J = 7.8 Hz, 2H), 7.20 (t, J = 7.7 Hz, 2H), 7.10 (d, J = 2.2 Hz, 4H), 7.08 (d, J = 2.3 Hz, 4H), 6.90 (dd, J = 8.2, 4.6 Hz, 2H), 6.59 (dd, J = 4.7, 1.3 Hz, 2H), 6.36 (s, 2H), 6.34 (s, 2H), 2.78 (hept, J = 6.9 Hz, 4H), 2.62 (hept, J = 6.8 Hz, 4H), 1.55 (d, J = 6.8 Hz, 12H), 1.11 (d, J = 6.9 Hz, 12H), 1.09 (d, J = 6.9 Hz, 12H), 1.05 (d, J = 6.9 Hz, 12H). ^{13}C NMR (151 MHz, C_6D_6, δ): 177.14, 146.08, 145.97, 141.36,

dx.doi.org/10.1021/ja4073832 | J. Am. Chem. Soc. 2013, 135, 16175−16183

136.23, 135.55, 133.60, 131.74, 130.46, 130.32, 130.01, 128.35, 124.43, 124.28, 122.47, 122.37, 118.79, 29.15, 29.02, 25.03, 24.91, 24.08, 23.68. Anal. calcd for $(C_{62}H_{70}N_6O_2Cu_2)\cdot 2(DMSO)\cdot 0.28(DME)$ (note: the ratio of **9** to DMSO and DME crystallization solvents was determined by integration of the ^1H NMR spectrum of elemental analysis sample): C, 65.91; H, 7.22; N, 6.48. Found: C, 65.28; H, 7.30; N, 6.49. IR (nujol mull): ν(C=O) 1540 cm^{-1}.

Synthesis of ***10***. In the glovebox, to an off-white suspension of 512 mg (1.65 mmol) of 4-methyl-4,5-diazafluorene iodide in 25 mL of THF was added a KO*t*Bu solution consisting of 186 mg (1.66 mmol) of KO*t*Bu dissolved in 25 mL of THF, this gave a royal blue solution along with a white suspension of KI. The mixture was left to stir at RT overnight, afterward the suspension was filtered through Celite, and the solvent was removed under high vacuum to give very dark blue crystals (297 mg, 98% yield). Crystals of **10** suitable for X-ray crystallographic analysis were grown via slow evaporation of a hexanes solution. Peaks of ^1H and ^{13}C NMR were assigned from select 2D NMR experiments; see Chart 1 for labeling scheme. ^1H NMR (400 MHz, DMSO-d_6, δ): 8.42 (dt, J = 8.1, 0.7 Hz, 1H, $\underline{H}_d$), 8.32 (dd, J = 4.0, 1.6 Hz, 1H, $\underline{H}_a$), 8.16 (dt, J = 5.6, 0.8 Hz, 1H, $\underline{H}_f$), 8.04 (dd, J = 8.5, 1.6 Hz, 1H, $\underline{H}_c$), 7.31 (dd, J = 8.2, 5.6 Hz, 1H, $\underline{H}_e$), 7.15 (dd, J = 8.5, 4.0 Hz, 1H, $\underline{H}_b$), 6.42 (s, 1H, $\underline{H}_g$), 4.97 (s, 3H, $\underline{H}_h$). ^{13}C NMR (101 MHz, DMSO-d_6, δ): 138.21 ($\underline{C}_1$), 131.37 ($\underline{C}_4$), 130.68 ($\underline{C}_8$), 130.41($\underline{C}_5$), 129.40 ($\underline{C}_7$ and $\underline{C}_{10}$ overlap), 126.55 ($\underline{C}_3$), 122.78 ($\underline{C}_6$), 118.16 ($\underline{C}_2$), 112.93 ($\underline{C}_9$), 84.01 ($\underline{C}_{11}$), 44.63 ($\underline{C}_{12}$).

Chart 1. NMR Peaks Assignment, Labelling Scheme for Compounds 10 (left) and 11 (right)

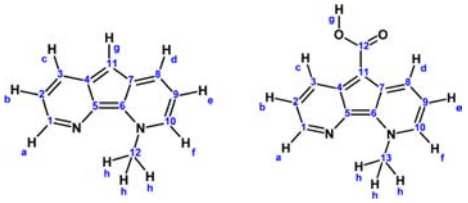

Synthesis of ***11***. In the glovebox, 123 mg (0.675 mmol) of **10** was dissolved in 18 mL of DME to give a deep blue-purple solution which was placed inside a Pyrex solvent bomb with resealable Teflon valve and removed from the glovebox. The mixture was degassed via two freeze–pump–thaw cycles, and then CO_2 was introduced while the bomb was submerged in a −78 °C dry ice cold bath. The bomb was then sealed, and left to sit in the cold-bath with no stirring to slowly warm to RT overnight. After warming to RT copious amounts of red-orange microcrystalline solids precipitated out of solution, the bomb was brought back into the glovebox for workup where it was degassed briefly by opening to vacuum. The red-orange precipitate was quickly collected by filtration, washed with hexanes, and dried under high vacuum for 8 h (124 mg, 76% yield based on **11**·0.16(DME), ratio of **11** to DME was determined by integration of ^1H NMR spectrum). Crystals of **11** suitable for X-ray crystallographic analysis were grown under CO_2 from DME, by allowing CO_2 to diffuse slowly into a septum-sealed vial containing a DME solution of **10** kept at ∼4 °C. For NMR characterization of **11** a 16 mg sample of **10** was dissolved in 0.6 mL of DMSO-d_6 to give a royal blue solution which was placed inside a J. Young NMR tube. The solution was degassed by two freeze–pump–thaw cycles, and then 1 atm of CO_2 was admitted into the J. Young tube. There was no immediate visible color change after introducing CO_2 at RT, the solution was then frozen in an ice water bath and left to thaw resulting in a pink solution of **11**. ^1H and ^{13}C NMR characterizations were done under an atmosphere of CO_2. Peaks of ^1H and ^{13}C NMR were assigned from select 2D NMR experiments; see Chart 1 for labeling scheme. ^1H NMR (400 MHz, DMSO-d_6, δ) 11.14 (s, 1H, $\underline{H}_g$), 9.10 (d, J = 8.2 Hz, 1H, $\underline{H}_d$), 8.65 (dd, J = 8.5, 1.7 Hz, 1H, $\underline{H}_c$), 8.47 (dd, J = 4.2, 1.6 Hz, 1H, $\underline{H}_a$), 8.43 (d, J = 5.6 Hz, 1H, $\underline{H}_f$), 7.62 (dd, J = 8.3, 5.7 Hz, 1H, $\underline{H}_e$), 7.39 (dd, J = 8.4, 4.2 Hz, 1H, $\underline{H}_b$), 4.99 (s, 3H, $\underline{H}_h$). ^{13}C NMR (101 MHz, DMSO-d_6, δ) 166.94 ($\underline{C}_{12}$), 140.63 ($\underline{C}_1$), 134.57 ($\underline{C}_5$), 133.60 ($\underline{C}_4$), 133.24 ($\underline{C}_{10}$), 132.74 ($\underline{C}_8$), 132.66 ($\underline{C}_6$), 127.70 ($\underline{C}_3$), 124.18 ($\underline{C}_7$), 120.99 ($\underline{C}_2$), 117.33 ($\underline{C}_9$), 87.10 ($\underline{C}_{11}$), 45.05 ($\underline{C}_{13}$). Anal. calcd for $(C_{13}H_{10}N_2O_2)\cdot 0.16(DME)$: C, 68.04; H, 4.87; N, 11.61. Found: C, 68.31; H, 4.75; N, 12.09. IR (nujol mull): ν(C=O) 1602 cm^{-1}.

X-ray Crystallography. The X-ray diffraction data were collected on a Bruker Kappa Apex II diffractometer and processed with the Bruker Apex 2 software package.[71] Data were collected with graphite monochromated Mo Kα radiation (λ = 0.71073 Å), at 150 K controlled by an Oxford Cryostream 700 series low-temperature system. The structures were solved by the direct methods or Patterson method and refined using SHELX-2013.[72] The residual electron density from disordered DMSO and benzene solvent molecules in the lattice of **9** was removed with the SQUEEZE function of PLATON,[73] and their contributions were excluded in the formula. The disordered IPr ligand and Cu2 in complex **9** were successfully modeled over two positions. Non-hydrogen atoms were refined anisotropically except for disordered portions. The hydrides in complex **4** were located directly from the difference Fourier map, while all other hydrogen atoms were calculated using the riding model. The position of the H atom attached to the carboxylic acid group of **4**, **8**, and **11** was calculated to fit with H-bonding patterns.

■ ASSOCIATED CONTENT

Ⓢ Supporting Information

CIF files for the X-ray structures of **4** and **6**–**11** along with NMR and IR spectra, TGA traces, and crystallographic data tables. This material is available free of charge via the Internet at http://pubs.acs.org.

■ AUTHOR INFORMATION

Corresponding Author

dsong@chem.utoronto.ca

Notes

The authors declare no competing financial interest.

■ ACKNOWLEDGMENTS

We thank the Natural Science and Engineering Research Council of Canada (NSERC) for funding. V.T.A. gratefully thanks the NSERC for a postgraduate scholarship (PGS D2) and the government of Ontario for an Ontario Graduate Scholarship (OGS). D.A.D. acknowledges NSERC for an Undergraduate Student Research Award (USRA). The authors also wish to acknowledge the Canadian Foundation for Innovation Project no. 19119 and the Ontario Research Fund for funding the CSICOMP NMR lab at the University of Toronto enabling the purchase of several new spectrometers.

■ REFERENCES

(1) Demessence, A.; D'Alessandro, D. M.; Foo, M. L.; Long, J. R. *J. Am. Chem. Soc.* **2009**, *131*, 8784–8786.

(2) Britt, D.; Furukawa, H.; Wang, B.; Glover, T. G.; Yaghi, O. M. *Proc. Natl. Acad. Sci. U.S.A.* **2009**, *106*, 20637–20640.

(3) Nune, S. K.; Thallapally, P. K.; McGrail, B. P. *J. Mater. Chem.* **2010**, *20*, 7623–7625.

(4) Phan, A.; Doonan, C. J.; Uribe-Romo, F. J.; Knobler, C. B.; O'Keeffe, M.; Yaghi, O. M. *Acc. Chem. Res.* **2010**, *43*, 58–67.

(5) Choi, H. S.; Suh, M. P. *Angew. Chem., Int. Ed.* **2009**, *48*, 6865–6869.

(6) In *Activation of Small Molecules: Organometallic and Bioinorganic Perspectives*; Tolman, W. B., Ed.; WILEY-VCH Verlag GmbH & Co. KGaA: Weinheim, 2006.

(7) Aresta, M.; Dibenedetto, A. *Dalton Trans.* **2007**, 2975–2992.

(8) Riduan, S. N.; Zhang, Y. *Dalton Trans.* **2010**, *39*, 3347–3357.

(9) Benson, E. E.; Kubiak, C. P.; Sathrum, A. J.; Smieja, J. M. *Chem. Soc. Rev.* **2009**, *38*, 89–99.

(10) Lewis, N. S.; Nocera, D. G. *Proc. Natl. Acad. Sci. U.S.A.* **2006**, *103*, 15729−15735.
(11) Sakakura, T.; Choi, J. C.; Yasuda, H. *Chem. Rev.* **2007**, *107*, 2365−2387.
(12) Askevold, B.; Roesky, H. W.; Schneider, S. *ChemCatChem* **2012**, *4*, 307−320.
(13) Grützmacher, H. *Angew. Chem., Int. Ed.* **2008**, *47*, 1814−1818.
(14) Gunanathan, C.; Milstein, D. *Acc. Chem. Res.* **2011**, *44*, 588−602.
(15) Gunanathan, C.; Milstein, D. *Top. Organomet. Chem.* **2011**, *37*, 55−84.
(16) van der Vlugt, J. I. *Eur. J. Inorg. Chem.* **2012**, 363−375.
(17) van der Vlugt, J. I.; Reek, J. N. H. *Angew. Chem., Int. Ed.* **2009**, *48*, 8832−8846.
(18) Annibale, V. T.; Song, D. *RSC Adv.* **2013**, *3*, 11432−11449.
(19) Braunstein, P.; Matt, D.; Dusausoy, Y.; Fischer, J.; Mitschler, A.; Ricard, L. *J. Am. Chem. Soc.* **1981**, *103*, 5115−5125.
(20) Braunstein, P.; Matt, D.; Nobel, D. *J. Am. Chem. Soc.* **1988**, *110*, 3207−3212.
(21) Braunstein, P.; Matt, D.; Nobel, D. *Chem. Rev.* **1988**, *88*, 747−764.
(22) Veya, P.; Floriani, C.; Chiesi-Villa, A.; Guastini, C.; Dedieu, A.; Ingold, F.; Braunstein, P. *Organometallics* **1993**, *12*, 4359−4367.
(23) Vogt, M.; Gargir, M.; Iron, M. A.; Diskin-Posner, Y.; Ben-David, Y.; Milstein, D. *Chem.—Eur. J.* **2012**, *18*, 9194−9197.
(24) Huff, C. A.; Kampf, J. W.; Sanford, M. S. *Organometallics* **2012**, *31*, 4643−4645.
(25) Vogt, M.; Rivada-Wheelaghan, O.; Iron, M. A.; Leitus, G.; Diskin-Posner, Y.; Shimon, L., J. W.; Ben-David, Y.; Milstein, D. *Organometallics* **2013**, *32*, 300−308.
(26) LeBlanc, F. A.; Berkefeld, A.; Piers, W. E.; Parvez, M. *Organometallics* **2012**, *31*, 810−818.
(27) Sgro, M. J.; Stephan, D. W. *Angew. Chem., Int. Ed.* **2012**, *51*, 11343−11345.
(28) Sgro, M. J.; Stephan, D. W. *Chem. Commun.* **2013**, *49*, 2610−2612.
(29) Chapman, A. M.; Haddow, M. F.; Wass, D. F. *J. Am. Chem. Soc.* **2011**, *133*, 18463−18478.
(30) Xu, X.; Kehr, G.; Daniliuc, C. G.; Erker, G. *J. Am. Chem. Soc.* **2013**, *135*, 6465−6476.
(31) Stepowska, E.; Jiang, H.; Song, D. *Chem. Commun.* **2010**, *46*, 556−558.
(32) Annibale, V. T.; Song, D. *Chem. Commun.* **2012**, *48*, 5416−5418.
(33) Jiang, H.; Stepowska, E.; Song, D. *Eur. J. Inorg. Chem.* **2009**, 2083−2089.
(34) Chiba, K.; Tagaya, H.; Karasu, M.; Ono, T.; Hashimoto, K.; Moriwaki, Y. *Bull. Chem. Soc. Jpn.* **1991**, *64*, 966−970.
(35) Chiba, K.; Tagaya, H.; Karasu, M.; Ono, T.; Saito, M.; Ashikagaya, A. *Bull. Chem. Soc. Jpn.* **1991**, *64*, 3738−3740.
(36) Chiba, K.; Tagaya, H.; Miura, S.; Karasu, M. *Chem. Lett.* **1992**, 923−926.
(37) Chiba, K.; Tagaya, H.; Karasu, M.; Ishizuka, M.; Sugo, T. *Bull. Chem. Soc. Jpn.* **1994**, *67*, 452−454.
(38) Tan, R.; Chiu, F. S. N.; Hadzovic, A.; Song, D. *Organometallics* **2012**, *31*, 2184−2192.
(39) Egbert, J. D.; Cazin, C. S. J.; Nolan, S. P. *Catal. Sci. Technol.* **2013**, *3*, 912−926.
(40) Zhang, L.; Hou, Z. *Chem. Sci.* **2013**, *4*, 3395−3403.
(41) Zhang, L.; Cheng, J.; Ohishi, T.; Hou, Z. *Angew. Chem., Int. Ed.* **2010**, *49*, 8670−8673.
(42) Boogaerts, I. I. F.; Fortman, G. C.; Furst, M. R. L.; Cazin, C. S. J.; Nolan, S. P. *Angew. Chem., Int. Ed.* **2010**, *49*, 8674−8677.
(43) Ohishi, T.; Nishiura, M.; Hou, Z. *Angew. Chem., Int. Ed.* **2008**, *47*, 5792−5795.
(44) Laitar, D.; Muller, P.; Sadighi, J. *J. Am. Chem. Soc.* **2005**, *127*, 17196−17197.
(45) Krylova, V. A.; Djurovich, P. I.; Whited, M. T.; Thompson, M. E. *Chem. Commun.* **2010**, *46*, 6696−6698.
(46) Hsu, S.; Li, C.; Chiu, Y.; Chiu, M.; Lien, Y.; Kuo, P.; Lee, H. M.; Huang, J.; Cheng, C. *J. Organomet. Chem.* **2007**, *692*, 5421−5428.
(47) Welle, A.; Diez-Gonzalez, S.; Tinant, B.; Nolan, S. P.; Riant, O. *Org. Lett.* **2006**, *8*, 6059−6062.
(48) Courtemanche, M.-A.; Légaré, M.-A.; Maron, L.; Fontaine, F.-G. *J. Am. Chem. Soc.* **2013**, *135*, 9326−9329.
(49) Bates, E.; Mayton, R.; Ntai, I.; Davis, J. *J. Am. Chem. Soc.* **2002**, *124*, 926−927.
(50) Wang, C.; Luo, X.; Luo, H.; Jiang, D.; Li, H.; Dai, S. *Angew. Chem., Int. Ed.* **2011**, *50*, 4918−4922.
(51) Duong, H. A.; Tekavec, T. N.; Arif, A. M.; Louie, J. *Chem. Commun.* **2004**, 112−113.
(52) Van Ausdall, B. R.; Glass, J. L.; Wiggins, K. M.; Arif, A. M.; Louie, J. *J. Org. Chem.* **2009**, *74*, 7935−7942.
(53) Kayaki, Y.; Yamamoto, M.; Ikariya, T. *Angew. Chem., Int. Ed.* **2009**, *48*, 4194−4197.
(54) Riduan, S. N.; Zhang, Y.; Ying, J. Y. *Angew. Chem., Int. Ed.* **2009**, *48*, 3322−3325.
(55) Jessop, P. G.; Mercer, S. M.; Heldebrant, D. J. *Energy Environ. Sci.* **2012**, *5*, 7240−7253.
(56) Gomes, C. D. N.; Jacquet, O.; Villiers, C.; Thuéry, P.; Ephritikhine, M.; Cantat, T. *Angew. Chem., Int. Ed.* **2012**, *51*, 187−190.
(57) Mömming, C. M.; Otten, E.; Kehr, G.; Fröhlich, R.; Grimme, S.; Stephan, D. W.; Erker, G. *Angew. Chem., Int. Ed.* **2009**, *48*, 6643−6646.
(58) Ashley, A. E.; Thompson, A. L.; O'Hare, D. *Angew. Chem., Int. Ed.* **2009**, *48*, 9839−9843.
(59) Berkefeld, A.; Piers, W. E.; Parvez, M. *J. Am. Chem. Soc.* **2010**, *132*, 10660−10661.
(60) Ménard, G.; Stephan, D. W. *Angew. Chem., Int. Ed.* **2011**, *50*, 8396−8399.
(61) Ménard, G.; Stephan, D. W. *J. Am. Chem. Soc.* **2010**, *132*, 1796−1797.
(62) Hounjet, L. J.; Caputo, C. B.; Stephan, D. W. *Angew. Chem., Int. Ed.* **2012**, *51*, 4714−4717.
(63) Jurkauskas, V.; Sadighi, J.; Buchwald, S. *Org. Lett.* **2003**, *5*, 2417−2420.
(64) Kaur, H.; Zinn, F. K.; Stevens, E. D.; Nolan, S. P. *Organometallics* **2004**, *23*, 1157−1160.
(65) Díez-González, S.; Escudero-Adán, E. C.; Benet-Buchholz, J.; Stevens, E. D.; Slawin, A. M. Z.; Nolan, S. P. *Dalton Trans.* **2010**, *39*, 7595−7606.
(66) Plater, M.; Kemp, S.; Lattmann, E. *J. Chem. Soc., Perkin Trans. 1* **2000**, 971−979.
(67) Thummel, R. P.; Lefoulon, F.; Mahadevan, R. *J. Org. Chem.* **1985**, *50*, 3824−3828.
(68) Kloc, K.; Mlochowski, J.; Szulc, Z. *Can. J. Chem.* **1979**, *57*, 1506−1510.
(69) Timpe, H. J.; Mlochowski, J.; Szulc, Z. *Z. Chem.* **1979**, *19*, 374−375.
(70) A small amount of an unidentified impurity was observed upon dissolving **4** (a sample that passed EA) in THF-d_8 and is also present after addition of CO_2 to the mixture of **3** and **4**. The $^1H\{^{31}P\}$ NMR spectrum shows a doublet at −16.84 ppm, and the ^{31}P NMR shows a doublet at 55.48 ppm belonging to the impurity. We speculate that this impurity may be a hydrido-formate complex resulting from insertion of CO_2 into the Rh-H, which would also have the same formula as compound **4**. There is also a broad peak at 8.64 ppm in the $^1H\{^{31}P\}$ NMR spectrum possibly belonging to the Rh-bound formate.
(71) *Apex 2 Software Package*; Bruker AXS Inc.: Fitchburg, WI, 2013.
(72) (a) Sheldrick, G. M. *Acta Crystallogr., Sect. A: Found. Crystallogr.* **2008**, *64*, 112. (b) *SHELX*; http://shelx.uni-ac.gwdg.de/SHELX/index.php (accessed July 4, 2013).
(73) Spek, A. L. *J. Appl. Crystallogr.* **2003**, *36*, 7.